





# Scaling machine learning-based chemical plant simulation: A method for fine-tuning a model to induce stable fixed points

Malte Esders <sup>a,b,\*</sup>, Gimmy Alex Fernandez Ramirez <sup>c,d</sup>, Michael Gastegger <sup>a,b</sup>, Satya Swarup Samal <sup>c,\*</sup>

<sup>a</sup>Machine Learning Group, Technische Universität Berlin, 10587 Berlin, Germany

<sup>b</sup>BASLEARN – TU Berlin/BASF Joint Lab for Machine Learning, Technische Universität Berlin, 10587 Berlin, Germany

<sup>c</sup>BASF SE, 67056 Ludwigshafen, Germany

<sup>d</sup>INEOS Styrolution Group GmbH, 67056 Ludwigshafen, Germany

---

## Abstract

Idealized first-principles models of chemical plants can be inaccurate. An alternative is to fit a Machine Learning (ML) model directly to plant sensor data. We use a structured approach: Each unit within the plant gets represented by one ML model. After fitting the models to the data, the models are connected into a flowsheet-like directed graph. We find that for smaller plants, this approach works well, but for larger plants, the complex dynamics arising from large and nested cycles in the flowsheet lead to instabilities in the cycle solver. We analyze this problem in depth and show that it is not merely a specialized concern but rather a more pervasive challenge that will likely occur whenever ML is applied to larger plants. To address this problem, we present a way to fine-tune ML models such that solving cycles with the usual methods becomes robust again.

*Keywords:* Machine Learning, Surrogate Model, Flowsheet Simulation, End-to-end training, Cycle Solving, Fixed point iteration, Cumene process, Digital twin





---

## 1. Introduction

Simulation is the default tool for planning and operating chemical plants. However, in addition to being time-consuming to set up, idealized simulations can give inaccurate results compared to the actual, brick-and-mortar plant. One of the reasons that the simulation might deviate from a real plant is that some

---

\*Corresponding author

*Email addresses:* [esders@tu-berlin.de](mailto:esders@tu-berlin.de) (Malte Esders ) , [gimmy.fernandez@ineos.com](mailto:gimmy.fernandez@ineos.com) (Gimmy Alex Fernandez Ramirez ) , [michael.gastegger@tu-berlin.de](mailto:michael.gastegger@tu-berlin.de) (Michael Gastegger ) , [satya-swarup.samal@basf.com](mailto:satya-swarup.samal@basf.com) (Satya Swarup Samal )

units of the plant may be too complex to be captured with equations, either because the exact equations are not known or because the full set of equations would be too large for a solver to converge. Another limitation is that existing simulation software cannot mathematically express each piece of equipment to the exact specifications. Additionally, time-based changes within the plant make the plant operation increasingly differ from the simulation (Bogojeski et al., 2021; Gordon and Pistikopoulos, 2022). Examples of such changes are catalyst degradation, the fouling of a heat exchanger, or the accumulation of byproducts. To achieve more accurate results, creating a model directly from sensor data is enticing, bypassing the above-mentioned limitations. Machine Learning (ML) is ideally suited for such a data-based modeling task.

Chemical plants can become highly complex, but this complexity arises by connecting a collection of much simpler units. In order to set up a simulation of a plant, all units are laid out on a 2D surface and are interconnected into a directed graph as required. The resulting graph is also called a flowsheet. It is possible to train an ML model which takes all the inputs to the flowsheet and predicts all outputs while ignoring the intermediate process units. We call such a model an *unstructured model*. However, we have chosen to use a *structured model* in which we model each process unit individually. Specifically, we model each process unit with a neural network (NN) and connect all NN models into an overall model representing the structure of the flowsheet (see fig. 1 for an illustration). The advantage of a structured over an unstructured model is having much finer-grained control over the internal processes. For instance, it becomes possible to answer questions like "What would happen if we increase the pressure after unit XYZ?".

Applications of ML models to chemical process engineering have been explored for several decades. The first studies comparable to ours were published by Palmer and Realf (2002a,b), who replaced units in the flowsheet simulation with polynomial and kriging models and performed optimization of the cost of operation. Recently, there has been a resurgence of interest in this topic (for an overview of recent progress see Lee et al. (2018); Schweidtmann et al. (2022)). ML models have been combined with physics-based equations for increased accuracy (Bikmukhametov and Jäschke, 2020), and have been used to optimize various units (Shalaby et al., 2021; Briceno-Mena et al., 2023) and entire flowsheets (Caballero and Grossmann, 2008; Burre et al., 2022). ML models have also been used to explore the solution space of flowsheet simulations (Heese et al., 2019; Ludl et al., 2022). An important emerging use-case for ML in chemical engineering which may benefit from the results of the current study is failure prediction for predictive maintenance of plants (Bogojeski et al., 2021; Gordon and Pistikopoulos, 2022).

Cycles in the flowsheet-graph are standard in chemical plants, e.g., due to recycling material from later stages in the process being fed back into the beginning of the plant or when using a heat exchanger. A nested cycle is present if at least one unit is part of two cycles simultaneously.

There are two common methods of solving flowsheets with cycles: *equation oriented* and *sequential modular*, or a hybrid of the two (Byrne and Bogle, 2000;

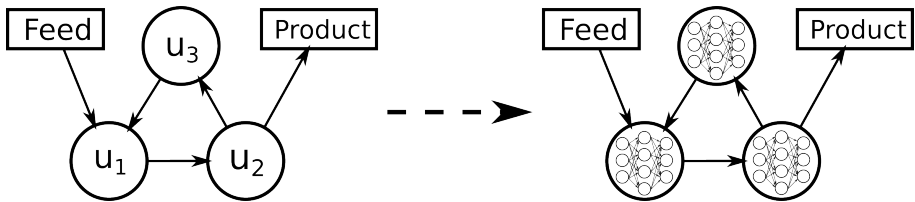


Figure 1: Left: Flowsheet schematic.  $u_1$ ,  $u_2$  and  $u_3$  are process units. The arrows indicate in which direction the chemicals flow. Right: In the present study, the first-principles-based simulation for each process unit is turned into an ML model, in this case, NNs.

Bongartz and Mitsos, 2019). The more common one is *equation oriented* solving (Shacham et al., 1982), where the equations governing each piece of equipment are solved simultaneously. Equation oriented solving is infeasible for ML-based models because the equations arising from the ML models are too complex to permit an analytic solution. Note that even for non-ML-based flowsheets, equation oriented solving does not always converge (Ishii and Otto, 2018; Ludl et al., 2022). Instead, ML-based structured models have to be solved in a *sequential modular* approach. In the sequential modular approach, one starts at the inputs to the flowsheet and computes the output of the first process unit. This output becomes the input to the next process unit, and so on.

A problem is encountered at the unit where a cycle stream terminates (fig. 3): values for the variables of the cycle stream are not known, therefore computing the output of that unit is not possible (see section 2.3 for a more thorough explanation). An initial guess for the cycle stream has to be used, and this initial guess is then refined iteratively. A plethora of cycle-solving algorithms have been published (Wegstein, 1958; Orbach and Crowe, 1971; Crowe and Nishio, 1975), however, as we show here, none of the solve methods we tested work well for solving ML-based cycles.

The initial guess in the cycle-solving procedure is not guaranteed to be close to the true values, which leads to problems with ML-based models: Since the initial guess is (typically) physically implausible, it has never been seen during training, and ML models do not always predict reasonable output values outside of their fitted input domain. These incorrect outputs are then propagated along the flowsheet, and with each prediction step, they deviate further from the true values.

When trying to apply previously published methods to a much larger, industrial-scale plant (the Cumene process), we found that the scaling-up is non-trivial because the challenges of the cycle-solving mentioned above become more severe and often prevent finding a solution. In this work, we start by showing that the presence of large and nested cycles leads to instabilities in all tested solve methods. We stress that these instabilities are not a niche problem of our particular example plant: Instead, such problems have to be expected whenever a plant contains large or nested cycles, as is common in chemical plants. In the next step, we propose a fine-tuning method to fix this problem. In this fine-tuning

method, there is a second training step, in which the ML models are changed slightly such that they predict more reasonable values (which are closer to the trained domain) even in the face of unrealistic input. We show qualitatively and quantitatively that after applying our proposed fine-tuning method, the solving of cycles becomes robust and trivial.

Our contributions in this study are as follows:

1. We extend existing approaches for structured modeling to significantly more complex processes. We provide a qualitative and quantitative analysis of existing approaches at this scale. In particular, we show that without modifications, established methods fail to produce partial models which are suitable for solving large or nested cycles.
2. We compare four different ways to solve cycles in ML-based flowsheet modeling: *direct substitution*, *Wegstein*, *Newton*, and *L-BFGS*.
3. We introduce a method that fine-tunes pretrained NN or other ML-based models such that all cycle solvers converge towards the true solution, even in the presence of nested cycles.

## 2. Methods

### 2.1. Synthetic model of Cumene process

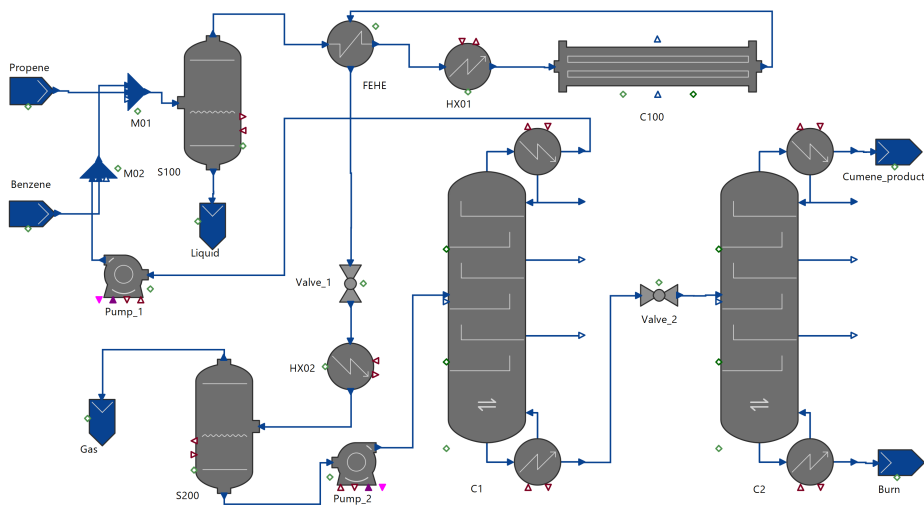


Figure 2: Cumene process flowsheet. For the type of each unit, refer to Table 2

As the basis for our experiments, we use the full Cumene process, which is a well-studied and complex process. The process model corresponds to the same used by Luyben (Luyben, 2010); kinetic data were taken from the same reference. Thermodynamic properties were estimated using the Redlich-Kwong-Suave equation of state provided by Multiflash (Multiflash Command Reference,

Infochem / KBC Advanced Technologies plc., Version 4.4, page 39) included in process simulation package gPROMS (Siemens Process Systems Enterprise Ltd. London, UK). Fig. 2 shows the flowsheet of the process.

A liquid mixture of 95 mol % propylene and 5 mol % of propane is mixed with a fresh stream of benzene and the recycled benzene coming from the first distillation column C1. The mixture is then fed to the S100 (a total evaporator) where it is evaporated, leaving S100 at 209°C and 25 bar. The vapors are then pre-heated using two heat exchangers: the first one, a feed-effluent heat exchanger (FEHE), uses part of the heat of the reactor’s effluent, the second, HX01, provides the additional heat to reach 360°C, which is the same temperature of the cooling medium of the reactor C100. C100 is a tubular reactor with 342 tubes, with 76.3 mm inside diameter, 2 mm wall thickness, and 6 m in length. It is filled with a solid catalyst of density 2000 kg/m<sup>3</sup> with a void fraction of 0.5 m<sup>3</sup>/m<sup>3</sup>. An overall heat transfer coefficient of the cooling of 65 W/m<sup>2</sup>K was used.

After the effluent is used to pre-heat the reactor’s feed, it is passed through Valve1 to reduce its pressure to 1.75 bar and cooled down to 90°C. The stream is now a liquid-vapor mixture that is separated in the flash tank S200. The liquid is then fed to the column C1. The column C1 has 15 stages; the feed is located in stage 8, and the average column pressure was specified to 1.75 bar, with a reflux ratio of 0.44 mol/mol. The purity of the Cumene at the bottom was specified to be 0,0005 mol/mol. The top effluent of the column, which is rich in benzene, is recycled. The Cumene-rich effluent of C1 is fed to the twelfth stage of the column C2. C2 has 20 stages and operates at an average pressure of 1 bar. Cumene was specified to be at most 0.001 mol/mol at the bottom, with a reflux ratio of 0.63 mol/mol.

## 2.2. Data generation procedure

In order to generate data to train the ML models, the Cumene process described in section 2.1 was simulated in various configurations. The simulation was run until it reached a steady-state for a given parameter combination. The following variables were captured in each stream after steady-state was reached: the total mass flowrate [kg/s], temperature [K], pressure [bar] and the chemical composition fractions [kg/kg]. The five chemicals involved are Benzene, Cumene, Diisopropylbenzene, Propane, and Propylene. All variables were measured both for the liquid and vapor phase (as long as each phase exists), such that in each stream, there were a maximum of 16 variables (otherwise 8 for just one phase).

For some types of equipment, there were additional variables: some types of equipment heat up the stream, in which case the heating power was captured as well [kW]. The distillation columns had the specified reflux ratio and rebound ratio [kg/kg] as additional inputs. Additionally, the output stream of the reactor C100 included the conversion of both Benzene and Propylene [kg/kg]. The data were generated by varying one variable of a small set of variables at a time and letting the simulation find appropriate values for all other variables.

Table 1 indicates the variables which were varied. We intentionally generated

| Variable                     | from | to   |
|------------------------------|------|------|
| Benzene inlet flow [kg/s]    | 1.18 | 2.68 |
| Propene inlet flow [kg/s]    | 1.08 | 1.45 |
| S100 output temperature [K]  | 440  | 512  |
| HX01 output temperature [K]  | 590  | 650  |
| Valve1 output pressure [bar] | 1    | 3    |
| HX02 output temperature [K]  | 353  | 373  |

Table 1: Ranges of variables that were varied to generate the data.

very few data points to best mimic real-world scenarios in which available data are typically limited. In total, 397 data points were created, of which 357 were used for training and 40 were used for testing.

### 2.3. Cycle solving

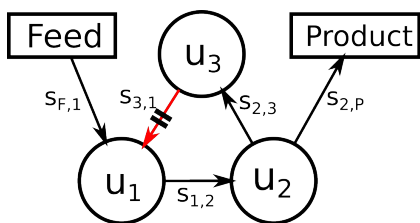


Figure 3: Flowsheet schematic with the tear stream indicated in red.

When propagating information between the nodes in the flowsheet, from the flowsheet input (Feed) to the output (Product), we assume that the only information given is the Feed. All other intermediate streams are considered unknown and must be predicted sequentially. In the presence of cycles however, this sequential procedure encounters a problem at the first unit where a cycle in the flowsheet terminates: As an example, take unit  $u_1$  (fig. 3). Let  $u_1(s_{F,1}, s_{3,1})$  also be the symbol for the function computing the output of unit  $u_1$ . While the input coming from Feed in stream  $s_{F,1}$  is known, the stream from  $u_3$ ,  $s_{3,1}$ , is not. Computing  $u_1(s_{F,1}, s_{3,1})$  is therefore impossible.

In order to find values for the streams along the cycle, an iterative cycle-solving procedure must be employed. The first step is to identify a *tear stream*. Any stream along a cycle can be chosen to be the tear stream. For the purpose of cycle solving, this tear stream is considered to be cut, thus breaking the cycle. An initial guess for the tear stream values is made, and with it, the rest of the streams along the cycle are predicted sequentially (black continuous arrows in the bottom part of fig. 4). Iteratively, the initial guess for the tear stream is improved every time the sequential prediction reaches the tear stream. Selecting a stream to be the tear stream is possible by visual inspection (by human designers) for simple flowsheets. For more intricate flowsheets, tear stream-finding algorithms exist (Pho and Lapidus, 1973).

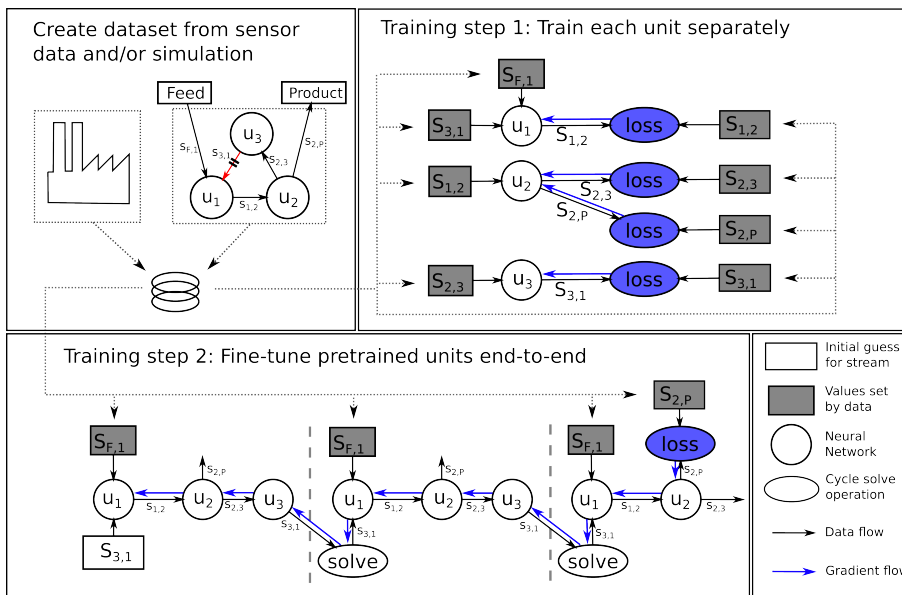


Figure 4: Top left: Data are generated either from sensors in a real plant, or from a first-principles-based simulation. Top right: The NN representing each flowsheet unit is trained individually, with each input/output set by the collected data. Bottom: The flowsheet is sequentially predicted from beginning to end, including the iterative cycle-solving (forward pass, black arrows). Afterward, the gradient is backpropagated through each node along the unrolled forward pass (blue arrows).

It is important to note that we consider the steady-state operation of a chemical plant. This means that all streams stay constant over time. When finding values for the tear stream, one needs to make sure that the obtained values maintain this steady-state. This means that when using the sequential modular approach to finding values for the tear stream, the estimate of the tear stream from one iteration needs to be equal to the next.

Mathematically, the iterative solving of a flowsheet cycle corresponds to fixed point iteration. Fixed point iteration is the repeated application of a function  $f$  to an initial value  $x_0$ .

$$\begin{aligned} x_1 &= f(x_0) \\ x_{k+1} &= f(x_k) \end{aligned} \quad (1)$$

Under certain conditions, the obtained sequence  $x_0, x_1, \dots, x_k$  is converging towards a fixed point. A fixed point is found if for some  $k$  the function value  $f(x^*)$  is equal to  $x^*$  itself:

$$x^* = f(x^*) \quad (2)$$

To see that solving a cycle in a flowsheet is equivalent to fixed-point iteration, we consider the cycle in fig. 3. In order to simplify the notation, we ignore the streams to and from the flowsheet,  $s_{F,1}$  and  $s_{2,F}$ . Applying the units  $u_1$ ,  $u_2$  and  $u_3$  to an initial guess for the stream  $s_{3,1_0}$  can be seen as a function composition

$f = u_3 \circ u_2 \circ u_1$ . The function  $f$  is called the *flowsheet response*. A flowsheet response function for an example cycle is displayed in fig. 5.

Repeated iteration through the cycle is equivalent to repeated application of the flowsheet response function and is, therefore, a fixed point iteration:

$$\begin{aligned} s_{3,1_{k+1}} &= u_3 \circ u_2 \circ u_1(s_{3,1_k}) \\ s_{3,1_{k+1}} &= f(s_{3,1_k}) \end{aligned} \quad (3)$$

### 2.3.1. Cycle solving methods used in this study

We compare four ways of solving nested cycles. The first method is the well-known and obvious *direct substitution* method (Smith, 2005), which works simply by using the flowsheet response for the tear stream as the new guess for the next iteration:

$$x_{k+1} = f(x_k) \quad (\text{direct substitution})$$

Applying the direct substitution method is visualized in fig. 5 (left). Each successive new estimate looks like a jump to the diagonal line where  $f(x_k) = x_k$ , resulting in the characteristic "staircase" plot. Note that for the initial value in the orange line, the iteration diverges towards infinity. In general, the direct substitution method, which is a fixed-point iteration, can only be guaranteed to converge to a unique fixed point if  $f$  is a "contraction mapping", which is equivalent to saying that  $f$  is Lipschitz continuous with Lipschitz constant  $K < 1$  (Banach fixed-point theorem (Banach, 1922)). For a differentiable function  $f : \mathbb{R} \rightarrow \mathbb{R}$ , such a condition (contraction mapping) is fulfilled if  $\sup |f'(x)| < 1$ . Despite this, the direct substitution method proved to be a surprisingly robust method for smaller cycles in our experiments.

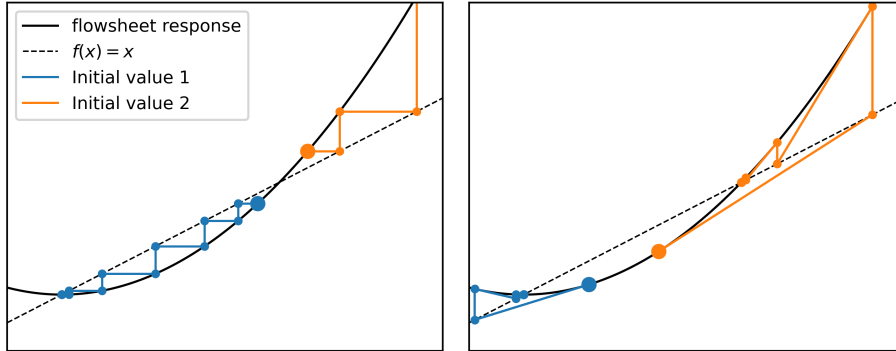


Figure 5: Visualization of a flowsheet response function and corresponding solve iterations of two different solve methods. The intersections of the flowsheet response curve (solid line) and the diagonal line where  $f(x) = x$  (dotted line) are the fixed points of the flowsheet response function. Left: Direct substitution method. Right: Newton method. The blue and orange lines represent iterations for different initial values. The initial values were chosen for illustrative purposes. Each solve iteration starts at the large circles.



The second method we compare is the *Wegstein* method (Wegstein, 1958). It is similarly well-known in the chemical process engineering literature (Smith, 2005) and is a method that can find a solution even in a locally divergent sequence. Also, like the direct substitution method, it does not need gradient information, although it uses an approximation to the gradient:

$$a = \frac{f(x_k) - f(x_{k-1})}{x_k - x_{k-1}} \quad (4)$$

Using  $a$ , the update in the Wegstein method is:

$$x_{k+1} = \frac{a}{a-1}x_k - \frac{1}{a-1}f(x_k) \quad (\text{Wegstein})$$

The third and fourth methods we compare are gradient-based methods. An advantage of using NNs is that the gradient is easily available, which enables us to use these methods. The arguably most obvious gradient-based method is the *Newton* root finding method. It can be seen that cycle solving is equivalent to root finding by a simple transformation of equation 2:

$$0 = f(x^*) - x^* \quad (5)$$

Therefore we are searching for the roots of a function  $F(x) = f(x) - x$ . In the Newton method, the iteration towards the root is given by

$$x_{k+1} = x_k - \frac{f(x_k)}{f'(x_k)} \quad (\text{Newton})$$

The resulting solve iteration of the Newton method is visualized in fig. 5 (right). If the gradient  $f'(x_k)$  is close to 1, the Newton method can select points far away for  $x_{k+1}$  (orange line), but in general it finds fixed points much faster than direct substitution.

The fourth method is the Broyden–Fletcher–Goldfarb–Shanno algorithm (*BFGS*) (Fletcher, 2013). The BFGS algorithm uses an approximation to the Hessian matrix  $B_k$  for finding the search direction  $p_k$  along which the next estimate  $x_{k+1}$  is searched. The search direction is the solution of  $B_k p_k = -f'(x_k)$ . After finding an appropriate step size  $\alpha_k$  along  $p_k$ , the update in the BFGS method is

$$x_{k+1} = x_k + \alpha_k p_k \quad (\text{BFGS})$$

#### 2.4. Training step 1: Single-unit neural network training

The method presented in this study involves two training steps (fig. 4). In the first training step, each NN was trained on its own. In the second training step, the entire flowsheet was fine-tuned end-to-end (see section 2.5). For the first training step, the data for the input and output streams belonging to the unit represented by a given NN were extracted from the data, and the NN was trained in the typical ML fashion to predict the output based on the input.

The NN architecture was two hidden layers with 100 neurons each. A skip connection in the form of a dense layer without an activation function from the input to the output was used. The activation function of the hidden layers was the *Softplus* function. Before forwarding through a NN, the input was normalized by subtracting the data mean and dividing by the standard deviation. The output of each NN was reverse-normalized again with the mean and standard deviation of the output stream. This enabled the NN to work with and predict values in reasonable data ranges and proved crucial for obtaining a good performance. For more training details, see Appendix A.

### 2.5. Training step 2: fine-tuning through the cycle solver

During inference, while using a solver to find solutions for the cycles in the flowsheet, the partial models are exposed to inputs that are not (necessarily) physically plausible. Consider unit  $u_1$  in fig. 3. The partial model for unit  $u_1$  receives input in stream  $s_{F,1}$ , and in stream  $s_{3,1}$  it receives the initial guess for the tear stream (typically the training dataset mean). Since the initial guess is not related to the new input, this combination of new input and initial guess is (typically) not physically plausible, and therefore the model for  $u_1$  has not been exposed to such combined input in its fitting procedure in training step 1. Since the partial models are not fitted in this domain, the gradients point in diverging directions and prevent the solver from converging (see section 3.3.1). We found that the fixed points of the nested cycles can be changed and improved when performing full end-to-end training through all solve iterations. It is possible to set up the cycle-solving programmatically such that a continuous gradient path exists from the beginning to the end, unrolling all intermediate cycle-solving steps in between (fig. 4). We call this method fine-tuning, as it only changes the pre-trained partial models slightly, just enough such that the fixed point moves towards the correct solution.

It is known that ML models often have unexpected gradients outside of their trained domain (Snyder et al., 2013; Schmitz et al., 2022). Backpropagating through a different type of solver has been attempted before: In Neural Ordinary Differential Equations (Neural ODEs), backpropagation is performed through the ODE solver (Chen et al., 2018). In Deep Equilibrium Models (DEQ), weight-tied NNs are trained such that from the fixed points of their hidden state the desired target can be calculated easily (Bai et al., 2019).

Our approach is similar: We compute a loss (and perform the according weight update) for the stream after each unit instead of just the flowsheet output, such that the intermediate predictions ideally don't become worse during fine-tuning (note that fig. 4 only shows loss computation after the final output stream for better readability). Additionally, we compute a loss after several different amounts of solve iterations. In particular, we first perform 0 solve iterations (using just the initial guesses) and then compute a loss after each unit. Then, in the next forward pass, we perform one solve iteration and again compute the loss after each unit. And so on, for all solve iterations between 0 and 10. Using all solve iterations between 0 and 10 was a design choice and one might as well use less or more. In our experiments, using a range of solve iterations instead

of just one had a considerable effect on the result (section 3.3 shows results for three different scenarios).

The overall loss for stream  $s$  after performing  $k$  solve iterations is

$$\mathcal{L}^{(k,s)} = \mathbb{E}_{x^{(s)}} \left[ (\hat{x}_k^{(s)} - x^{(s)})^2 \right] \quad (6)$$

where  $\hat{x}_k^{(s)}$  is the value for the prediction of stream  $s$  and solve iteration  $k$ , and  $x^{(s)}$  is the true value for this stream. Taking into account that in our case each stream is predicted by a series of NNs whose parameters we group into a vector  $\theta$ , the full loss gradient with which to perform the fine-tuning becomes

$$\frac{\partial \mathcal{L}^{(k,s)}}{\partial \theta} = \sum_{i=0}^k \frac{\partial \mathcal{L}^{(k,s)}}{\partial \hat{x}_i^{(s)}} \frac{\partial \hat{x}_i^{(s)}}{\partial \theta}$$

The summation over loss iterations in the formula for the loss gradient is because the computation of the value  $x_i^{(s)}$  in each iteration  $i \in 0, \dots, k$  contributes to the final value of  $\hat{x}_k^{(s)}$  and therefore to the loss and gradient. After summing the gradients from all amounts of solve iterations, the full gradient update becomes

$$\Delta \theta = \eta \frac{1}{K} \frac{1}{S} \sum_{k=0}^K \sum_{s=0}^S \frac{\partial \mathcal{L}^{(k,s)}}{\partial \theta} \quad (7)$$

where  $\eta$  is the learning rate and we normalize by the total number of solve iterations and the number of streams.

### 3. Results

#### 3.1. Single unit and small cycle

In order to show that failures during the cycle solving were not due to the single unit models, we first present results for the single unit prediction and for a small cycle within the Cumene process (fig. 2).

The most complex process unit in the flowsheet is the reactor C100. Even for the C100, the predictions are almost perfect (fig. 6). Notice that the near-perfect accuracy was only achievable because we are using simulated data as a substitute for real-world plant sensor data. The predictions for all other units were similarly good (see table 2). Based on this near-perfect accuracy on the single-unit prediction, one would expect that combining all single-unit ML models into a full "flowsheet" would yield similarly good results on the end-to-end prediction task.

Since all training data are from the steady-state operation of the plant (see section 2.2), one can only expect good prediction accuracy in steady-state conditions. During the cycle solving, however, the system is not yet in the steady-state. In particular, when injecting an initial guess for the tear stream (as an example, stream  $s_{3,1}$  in fig. 3), this initial guess is not in steady-state in connection with the flowsheet inputs (hence that the cycle solving is necessary in the

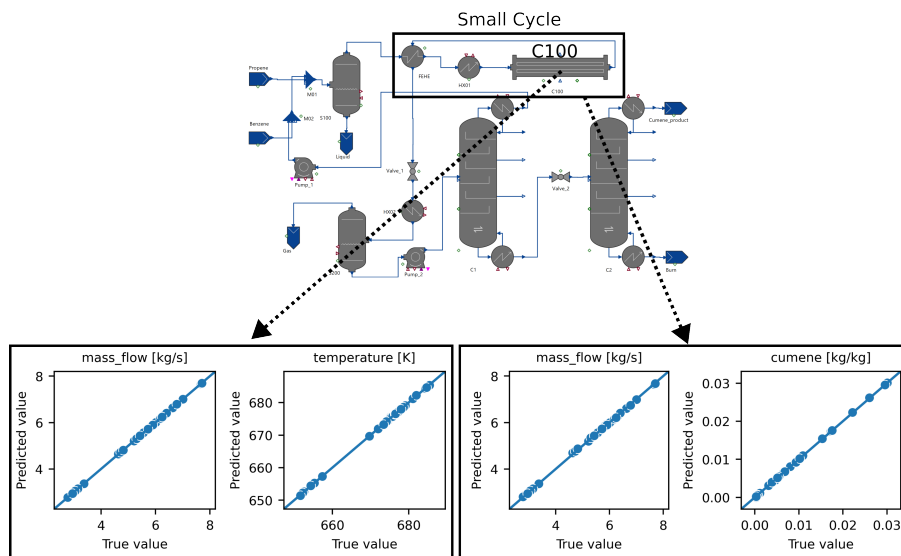


Figure 6: Top: position of the C100 (reactor) and the "small cycle". Bottom left: Parity plot for the single-unit prediction of the C100 reactor. Bottom right: Parity plot for the propagation through the small cycle, including iteratively improving the estimate from initial values. The second variable shown is Cumene and not Temperature, because the temperature is constant at the outlet of the FEHE heat exchanger.

first place). Therefore, this combination of flowsheet input and recycle-stream-initial-guess has not been seen during single-unit training.

It is not immediately clear whether a model that is only fitted to steady-state conditions performs well enough outside of the steady-state such that cycle-solving is still possible.

As a first experiment with cycle solving with ML-based models, we tried to solve the small cycle in fig. 6 (for a larger version of the flowsheet see fig. 2). The cycle was extracted from the Cumene process flowsheet and treated as an independent flowsheet.

The three units *FEHE*, *HX01* and *C100* were trained independently (single-unit training, training step 1 in fig. 4). After training each of the three units, the models were connected to obtain one overall model representing the entire flowsheet. The input to this new flowsheet is the non-cycle input to the *FEHE* heat exchanger unit (the *FEHE* has two inputs, the other being the tear stream coming from *C100*). We tried cycle-solving methods as introduced in sec. 2.3.1 to solve this cycle. All four methods behaved almost exactly the same and converged towards the same (correct) value (fig. 6), therefore per-method results are not shown here.

### 3.2. Full flowsheet before fine-tuning

The fact that the small cycle with ML-based units could be solved with established cycle-solving techniques was expected based on previous studies (Palmer and Realf, 2002a; Bubel et al., 2021). We tried the same technique on the entire flowsheet, which contains a larger cycle and the smaller cycle nested within this larger cycle. The scalar error we report for the full flowsheet is measured as the mean standard deviation-scaled difference between the true values and the prediction at the top output of the C2 column. This output is the one that produces the Cumene and therefore is the most relevant.

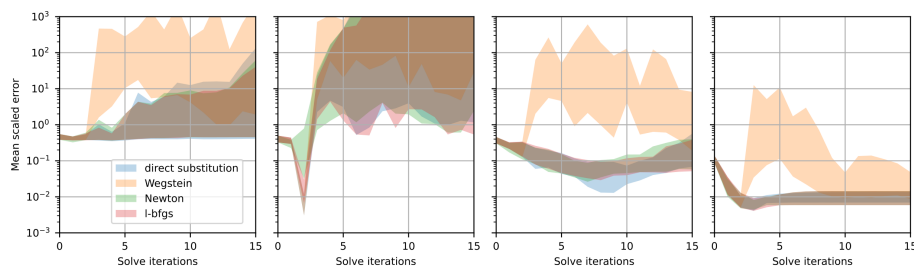


Figure 7: Solving the full flowsheet (with both cycles). The y-axis represents the mean, standard deviation-scaled error of the prediction of the C2-top output. The ranges represent the 25th to 75th percentile across identical runs. Left: Without fine-tuning. Center left: fine-tuning only for  $K = 2$  solve iterations. Center right: fine-tuning for  $K = 10$  solve iterations. Right: fine-tuning for  $K = \{0, 1, 2, \dots, 10\}$  solve iterations.

Unlike the results from solving just the small cycle, where established cycle-solving techniques worked well, the same techniques did not work for the full flowsheet (fig. 7 left). With an increasing number of solve iterations, the predictions became worse, in other words, the solving procedure diverged. A qualitative analysis of the solving behavior revealed that divergence happens especially in regions of the data space where not much data was available (section 3.3.1). What was surprising was that all four examined cycle-solving methods performed similarly. The Wegstein method is usually regarded as a particularly stable method, but in our experiments the opposite was true. The Wegstein method typically performed worse than the other methods, and its variability between experiments was high.

### 3.3. Full flowsheet after fine-tuning

The instabilities of the cycle-solving methods can be avoided by using the fine-tuning method introduced in this study (Training step 2, see section 2.5). It is important not to confuse solve iterations during *training* (for fine-tuning, as shown in fig. 4 bottom), and during *prediction* of the test data for evaluation. The fine-tuning can be done for a fixed number of total solve iterations  $K$ , or for several different values of  $K$ . For instance, we can do fine-tuning with  $K = 2$ . What that means is that during fine-tuning, we alternate between doing

a forward pass through the flowsheet, including going through the cycle 2 times, and doing a backward pass as indicated in fig. 4.

For the result of performing fine-tuning with  $K = 2$  and  $K = 10$ , see fig. 7 center left and center right. Note that the solve iterations on the x-axis correspond to the *prediction* solve iterations. We can also set  $K$  to a list of values, for instance  $K = \{0, 1, 2, 3, \dots, 10\}$ . In this case, we repeatedly iterate between each value of  $K$  and perform one fine-tuning iteration with each  $K$ . We found that doing fine-tuning for several total solve iterations iteratively worked best (fig. 7 right). Interestingly, if fine-tuning is only done for a specific number of solve iterations, the prediction works best for that number of solve iterations too. For instance, in the case  $K = 2$  during fine-tuning, the *prediction* with 2 solve iterations worked best (fig. 7 center left). This was not the case anymore when doing fine-tuning with 10 solve iterations, however (fig. 7 center right). After fine-tuning in the  $K = 0, 1, 2, \dots, 10$  condition, predictions were near-perfect (fig. 8). Fine-tuning for the results in fig. 7 was always done with the direct substitution method, regardless of the prediction solve method, because it worked the best, but see the appendix Appendix B for all combinations of solve methods for training and prediction.

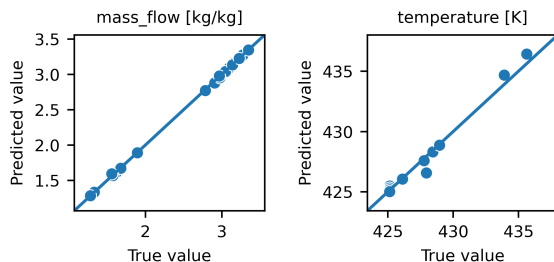


Figure 8: Parity plot of the end-to-end prediction of the entire flowsheet after fine-tuning.

### 3.3.1. Phase portrait of cycle solving

To further illustrate the difference in the flowsheet response before and after fine-tuning, we display a phase portrait in fig. 9. The arrows indicate the direction in which the cycle estimate moves if one solve iteration is performed. The origin of the arrow indicates the two values of temperature and Cumene concentration which are substituted into the initial guess for the cycle. The head of the arrows indicates the direction in which these two values move after one cycle iteration. The blue dots in fig. 9 indicate the data points of the training set.

The data distribution looks unusual compared to familiar ML datasets due to the fact that in the simulation for the data generation, only a narrow range of values is permissible. Note that for lower temperatures, there were fewer data points than at higher temperatures, which probably led to a worse fit of the models in this region.

After fine-tuning, it can be seen that the values do not diverge anymore, but

that from all locations in the diagram, the values converge towards the correct solution (green  $X$  in the figure). The background color of fig. 9 indicates the standard deviation-scaled mean square loss of the tear stream after one iteration. In the left plot, representing the model before finetuning, it can be seen that large regions of the domain lead to a huge loss, whereas the opposite is true after finetuning, where starting from almost any point in the domain, the resulting loss is very small.

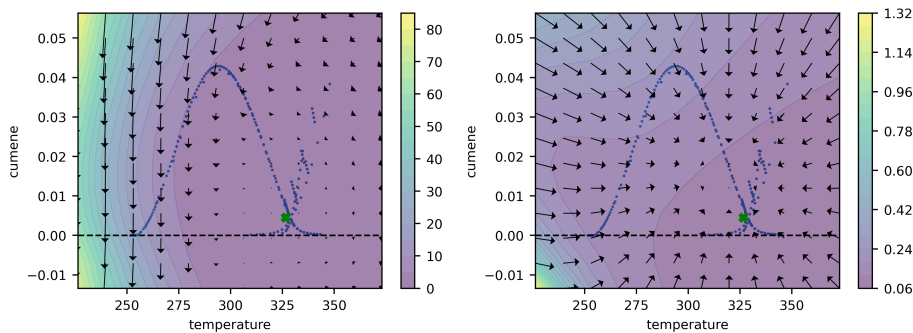


Figure 9: Phase portrait of temperature [K] and Cumene content [kg/kg]. Arrows indicate the direction toward the new predictions of the tear stream after propagation through the cycle. The green star indicates the true value for the cycle. The background color indicates the standard deviation-scaled mean squared error of the cycle estimate. Left: Before fine-tuning. Right: After fine-tuning.

### 3.3.2. Fine-tuning impact on single-unit accuracy

An interesting question is whether the single-unit accuracy gets impeded by the fine-tuning. This would be a trade-off between single-unit accuracy and performance of the end-to-end prediction.

Table 2 shows the single-unit accuracy before and after fine-tuning. While most units had an almost negligible decrease in accuracy, the unit S100 is an exception and its  $r^2$ -value decreased from 0.999 to 0.585. We do not know why the unit S100 changed its prediction by so much while all other units are virtually unchanged. To further investigate, we performed another experiment. For training step 1, we proceeded as usual, but in training step 2, the fine-tuning was done with the weights of the S100 unit frozen. Table 2 shows the results of this experiment. As expected, the performance of the S100 unit is unchanged ( $r^2 = 0.999$  before and after fine-tuning), but interestingly, there is no one single unit that "takes over" the role of the S100 and significantly decreases in accuracy. The full-flowsheet predictions are still near-perfect even with the frozen S100 model included (results not shown, but almost indistinguishable from results in fig. 8). This indicates that the relatively large change in the S100 accuracy before was not necessary to induce stable and correct fixed points.

| Unit Name                | Unit Type           | After only<br>Training step 1 | After fine-tuning | After fine-tuning<br>with frozen S100 |
|--------------------------|---------------------|-------------------------------|-------------------|---------------------------------------|
| C1                       | Distillation column | 1.000                         | 0.997             | 0.996                                 |
| C100                     | Tubular reactor     | 0.999                         | 0.997             | 0.997                                 |
| C2                       | Distillation column | 1.000                         | 0.996             | 0.994                                 |
| FEHE                     | Heat exchanger      | 1.000                         | 0.984             | 0.970                                 |
| HX01                     | Heater              | 1.000                         | 0.997             | 0.996                                 |
| HX02                     | Cooler              | 1.000                         | 0.994             | 0.993                                 |
| M01                      | Mixer               | 1.000                         | 0.956             | <b>0.942</b>                          |
| M02                      | Mixer               | 0.999                         | 0.966             | 0.968                                 |
| Pump1                    | Pump                | 0.999                         | 0.995             | 0.994                                 |
| Pump2                    | Pump                | 1.000                         | 1.000             | 1.000                                 |
| S100                     | Separator           | 0.999                         | <b>0.585</b>      | 0.999                                 |
| S200                     | Separator           | 1.000                         | 0.999             | 0.999                                 |
| Valve1                   | Valve               | <b>0.998</b>                  | 0.975             | 0.978                                 |
| Valve2                   | Valve               | 1.000                         | 1.000             | 0.999                                 |
| End-to-end<br>prediction | Whole Flowsheet     | -0.806                        | 0.993             | 0.988                                 |

Table 2: The performance impact of fine-tuning on the single-unit and end-to-end prediction performance. The prediction accuracy is measured with the coefficient of determination ( $r^2$ ) before and after fine-tuning. Bold text indicates the lowest value per column (excluding end-to-end prediction). Note that the performance of the end-to-end prediction before fine-tuning varies (see fig.7).

#### 4. Discussion

The current study is the result of trying to apply published methods of ML-based chemical plant models to an industrial-scale example, in our case the Cumene process. It was found that published methods work well on smaller scales, but do not easily scale up. In particular, we noticed that in the presence of nested cycles, which are common in chemical process engineering, the cycle-solving operation runs into instabilities. All four cycle-solving methods we tested suffered from these instabilities. We hypothesized that these instabilities arise from the fact that during cycle-solving, the ML models are applied to input that is out of the training domain, a common problem whenever ML is applied to real-world systems (Leinen et al., 2020; Won et al., 2020).

To mitigate this problem, we introduce a method we call fine-tuning to condition the pre-trained networks such that cycle solving with classical methods works again. By backpropagating the training loss through the iterative solving procedure, we were able to tune the NNs ever so slightly such that the instabilities in the solving operation are overcome.

Looking ahead, the next obvious step is to apply our method to a real plant and to learn from sensor data. To do this, there is one hurdle: there won't be sensor data available for all intermediate values. Therefore, training the ML models as we did so far would not be possible. This problem can be overcome with a hybrid approach in which one trains from both simulated and sensor data. When



training with sensor data, error gradients can be generated from the variables available, and the other variables can be ignored. The simulated data are then used to train those variables for which no sensor data are available.

However, we also see a possible second application of the proposed fine-tuning method here: by letting the error gradient flow end-to-end, intermediate units for which data are not available can be learned implicitly. This only works if data for at most every second unit is missing. We defer the exploration of this idea to future work.

Another promising direction for future work is to use fine-tuned ML models for optimization. Mathematically, ML-based models have properties such as smoothness, no discontinuities, and availability of gradients which make them well-suited for optimization. Also, ML models are typically much faster to evaluate than solving first-principles-based equation systems. While we did not explore optimization with ML-based models in the current study, there is enormous research interest in this direction (Schweidtmann et al., 2018; Bradford et al., 2018; Asprión et al., 2019; Schweidtmann et al., 2019; Burre et al., 2022) and our proposed fine-tuning method might pave the way to optimization of larger and more complex plants.

In a nutshell, we show here that when extending structured ML-based plant simulation to industrial scales, existing methods run into instabilities, and one way to solve this problem is by fine-tuning the partial models end-to-end.

## Acknowledgements

ME and MG work at the BASLEARN-TU Berlin/BASF Joint Lab for Machine Learning, co-financed by TU Berlin and BASF SE. We thank Bruno Betoni Parodi for fruitful discussions and for managing BASLEARN.

## References

- Asprión, N., Böttcher, R., Pack, R., Stavrou, M.E., Höller, J., Schwientek, J., Bortz, M., 2019. Gray-box modeling for the optimization of chemical processes. *Chemie Ingenieur Technik* 91, 305–313.
- Bai, S., Kolter, J.Z., Koltun, V., 2019. Deep equilibrium models. *Advances in Neural Information Processing Systems* 32.
- Banach, S., 1922. Sur les opérations dans les ensembles abstraits et leur application aux équations intégrales. *Fundamenta mathematicae* 3, 133–181.
- Bikmukhametov, T., Jäschke, J., 2020. Combining machine learning and process engineering physics towards enhanced accuracy and explainability of data-driven models. *Computers & Chemical Engineering* 138, 106834.
- Bogojeski, M., Sauer, S., Horn, F., Müller, K.R., 2021. Forecasting industrial aging processes with machine learning methods. *Computers & Chemical Engineering* 144, 107123.

- Bongartz, D., Mitsos, A., 2019. Deterministic global flowsheet optimization: Between equation-oriented and sequential-modular methods. *AIChE Journal* 65, 1022–1034.
- Bradford, E., Schweidtmann, A.M., Lapkin, A., 2018. Efficient multiobjective optimization employing gaussian processes, spectral sampling and a genetic algorithm. *Journal of global optimization* 71, 407–438.
- Briceno-Mena, L.A., Arges, C.G., Romagnoli, J.A., 2023. Machine learning-based surrogate models and transfer learning for derivative free optimization of ht-pem fuel cells. *Computers & Chemical Engineering* 171, 108159.
- Bubel, M., Ludl, P.O., Seidel, T., Asprion, N., Bortz, M., 2021. A modular approach for surrogate modeling of flowsheets. *Chemie Ingenieur Technik* 93, 1987–1997.
- Burre, J., Kabatnik, C., Al-Khatib, M., Bongartz, D., Jupke, A., Mitsos, A., 2022. Global flowsheet optimization for reductive dimethoxymethane production using data-driven thermodynamic models. *Computers & Chemical Engineering* 162, 107806.
- Byrne, R., Bogle, I., 2000. Global optimization of modular process flowsheets. *Industrial & engineering chemistry research* 39, 4296–4301.
- Caballero, J.A., Grossmann, I.E., 2008. An algorithm for the use of surrogate models in modular flowsheet optimization. *AIChE journal* 54, 2633–2650.
- Chen, R.T., Rubanova, Y., Bettencourt, J., Duvenaud, D.K., 2018. Neural ordinary differential equations. *Advances in neural information processing systems* 31.
- Crowe, C.M., Nishio, M., 1975. Convergence promotion in the simulation of chemical processes—the general dominant eigenvalue method. *AIChE Journal* 21, 528–533.
- Fletcher, R., 2013. *Practical methods of optimization*. John Wiley & Sons.
- Gordon, C.A.K., Pistikopoulos, E.N., 2022. Data-driven and safety-aware holistic production planning. *Journal of Loss Prevention in the Process Industries* 77, 104754.
- Heese, R., Walczak, M., Seidel, T., Asprion, N., Bortz, M., 2019. Optimized data exploration applied to the simulation of a chemical process. *Computers & Chemical Engineering* 124, 326–342.
- Ishii, Y., Otto, F.D., 2018. Decoupling the constraints for process simulation in large-scale flowsheet optimization. *Computers & Chemical Engineering* 113, 240–252.
- Kingma, D.P., Ba, J., 2014. Adam: A method for stochastic optimization. *arXiv preprint arXiv:1412.6980* .

- Lee, J.H., Shin, J., Realf, M.J., 2018. Machine learning: Overview of the recent progresses and implications for the process systems engineering field. *Computers & Chemical Engineering* 114, 111–121.
- Leinen, P., Esders, M., Schütt, K.T., Wagner, C., Müller, K.R., Tautz, F.S., 2020. Autonomous robotic nanofabrication with reinforcement learning. *Science advances* 6, eabb6987.
- Ludl, P.O., Heese, R., Höller, J., Asprión, N., Bortz, M., 2022. Using machine learning models to explore the solution space of large nonlinear systems underlying flowsheet simulations with constraints. *Frontiers of Chemical Science and Engineering* 16, 183–197.
- Luyben, W.L., 2010. Design and control of the cumene process. *Industrial & engineering chemistry research* 49, 719–734.
- Orbach, O., Crowe, C., 1971. Convergence promotion in the simulation of chemical processes with recycle—the dominant eigenvalue method. *The Canadian Journal of Chemical Engineering* 49, 509–513.
- Palmer, K., Realf, M., 2002a. Metamodeling approach to optimization of steady-state flowsheet simulations: Model generation. *Chemical Engineering Research and Design* 80, 760–772.
- Palmer, K., Realf, M., 2002b. Optimization and validation of steady-state flowsheet simulation metamodels. *Chemical Engineering Research and Design* 80, 773–782.
- Pho, T., Lapidus, L., 1973. Topics in computer-aided design: Part i. an optimum tearing algorithm for recycle systems. *AIChE Journal* 19, 1170–1181.
- Schmitz, N.F., Müller, K.R., Chmiela, S., 2022. Algorithmic differentiation for automated modeling of machine learned force fields. *The Journal of Physical Chemistry Letters* 13, 10183–10189.
- Schweidtmann, A.M., Bongartz, D., Huster, W.R., Mitsos, A., 2019. Deterministic global process optimization: Flash calculations via artificial neural networks, in: *Computer Aided Chemical Engineering*. Elsevier. volume 46, pp. 937–942.
- Schweidtmann, A.M., Bongartz, D., Mitsos, A., 2022. Optimization with trained machine learning models embedded, in: *Encyclopedia of Optimization*. Springer, pp. 1–8.
- Schweidtmann, A.M., Clayton, A.D., Holmes, N., Bradford, E., Bourne, R.A., Lapkin, A.A., 2018. Machine learning meets continuous flow chemistry: Automated optimization towards the pareto front of multiple objectives. *Chemical Engineering Journal* 352, 277–282.

- Shacham, M., Macchieto, S., Stutzman, L., Babcock, P., 1982. Equation oriented approach to process flowsheeting. *Computers & Chemical Engineering* 6, 79–95.
- Shalaby, A., Elkamel, A., Douglas, P.L., Zhu, Q., Zheng, Q.P., 2021. A machine learning approach for modeling and optimization of a co2 post-combustion capture unit. *Energy* 215, 119113.
- Smith, R., 2005. *Chemical process: design and integration*. John Wiley & Sons.
- Snyder, J.C., Mika, S., Burke, K., Müller, K.R., 2013. Kernels, pre-images and optimization. *Empirical Inference: Festschrift in Honor of Vladimir N. Vapnik*, 245–259.
- Wegstein, J.H., 1958. Accelerating convergence of iterative processes. *Communications of the ACM* 1, 9–13.
- Won, D.O., Müller, K.R., Lee, S.W., 2020. An adaptive deep reinforcement learning framework enables curling robots with human-like performance in real-world conditions. *Science Robotics* 5, eabb9764.

## Appendix A. Training details

Each NN had two hidden layers with 100 neurons each, and a skip connection layer going directly from the input to the output. The activation function was the softplus in all cases:

$$a(x) = \log(1 + e^x) \quad (\text{A.1})$$

Single-unit training was done with the Adam optimizer (Kingma and Ba, 2014) with a learning rate of  $2.0e - 5$  for  $2e4$  epochs. Fine-tuning training was also done with the Adam optimizer, for 500 epochs with a learning rate of  $2.0e - 5$ . Input to each NN was normalized with the mean  $\mu$  and the standard deviation  $\sigma$ :

$$f_{normal}(x) = \frac{x - \mu}{\sigma} \quad (\text{A.2})$$

After prediction, the reverse of the normalizing operation was performed

$$f_{reverse}(x) = x * \sigma + \mu \quad (\text{A.3})$$

## Appendix B. Further fine-tuning results

It is possible to use a different solve method for training than for inference. In the main text, training was always done with the *direct substitution* method because it is the most robust. We show in fig. B.10 the results for all combinations of training and inference solve methods. The plots in the first column have no finetuning and therefore are runs with exactly the same parameters. The differences between the plots in the first column are therefore solely based on the random initialization of the NNs.

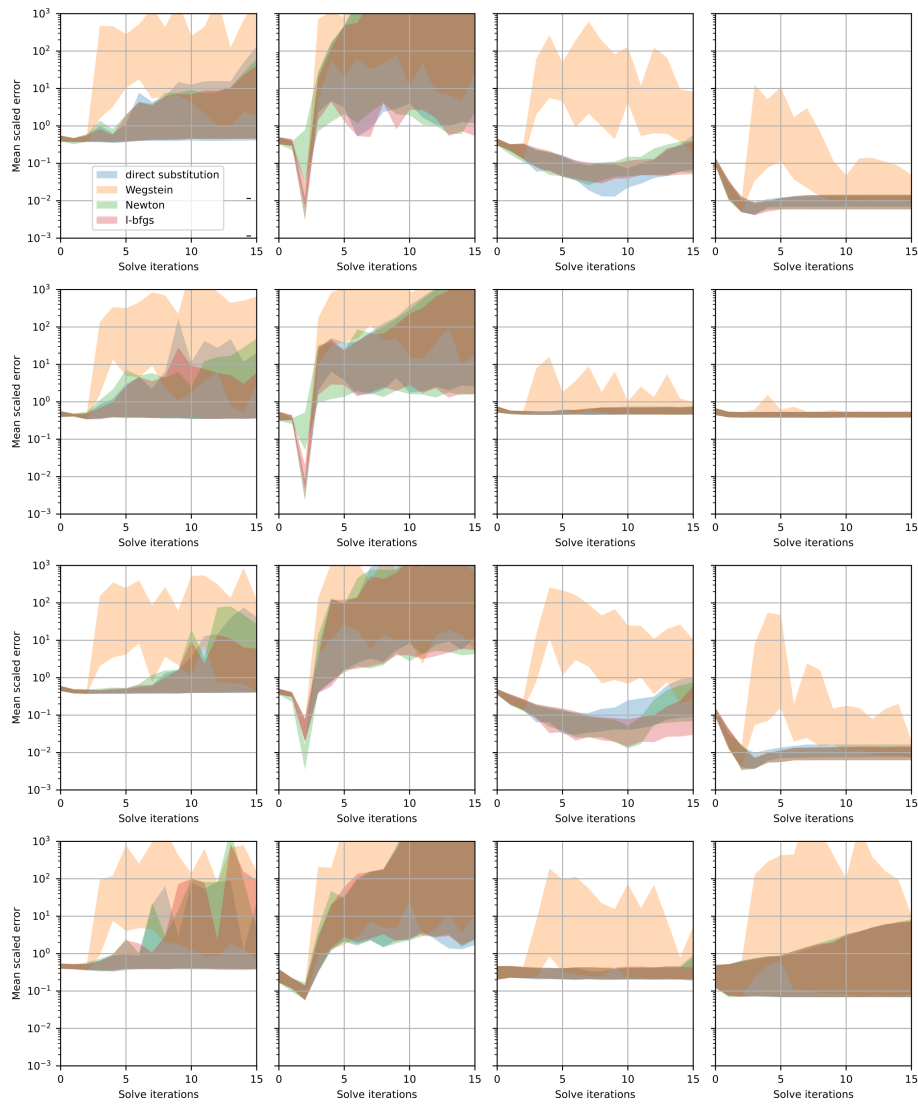


Figure B.10: Each row of plots corresponds to fine-tuning with one particular solve method, from top to bottom *direct substitution*, *Wegstein*, *Newton*, *L-BFGS*. Each column of plots corresponds to fine-tuning with the following fine-tuning conditions (left to right): *no fine-tuning*, *fine-tuning 2 solve iterations*, *fine-tuning 10 solve iterations*, *fine-tuning 0, 1, ..., 10 solve iterations*. The colors within each plot represent the solve method used for prediction (see the top left plot for a legend).